19th WORLD CONFERENCE OF THE ASSOCIATED RESEARCH CENTRES FOR THE URBAN UNDERGROUND SPACE
Belgrade, Serbia, November 4-7, 2025.

ACUUS BELGRADE 2025

Paper No: 2.4.38
DOI: 10.46793/ACUUS2025.2.4.38

RESEARCH ON THE HIGH-TEMPERATURE MECHANICAL PROPERTIES OF CORRUGATED STEEL-CONCRETE COMPOSITE STRUCTURES IN TUNNEL ENGINEERING UNDER FIRE

Bo Lei[1], Wenqi Ding[2], Qingzhao Zhang[3]

Abstract: Corrugated steel-concrete (CSC) composite structures have been increasingly applied in tunnel engineering due to their excellent mechanical properties. Due to the frequent occurrence of tunnel fires, accurately evaluating the high-temperature mechanical properties of CSC composite structures is crucial for determining the stability of lining structures under tunnel fires. This paper employs the novel S32001 duplex stainless steel to investigate the thermo-mechanical coupling of CSC composite structures through numerical simulation. The study explores the load-bearing capacity and deformation characteristics of CSC composite structures under various temperature conditions and the ISO 834 standard heating curve, while evaluating structural stability across different operating conditions. Research indicates that CSC composite structures exhibit similar deformation characteristics under temperature conditions ranging from 100 °C to 500 °C, with vertical displacement and stress levels increasing as temperature rises and time progresses. Under the ISO834 heating curve, corrugated steel plates heats up relatively quickly and the trough temperature is higher than the peak temperature. The temperature field distribution of the concrete in the cross-section of the specimen shows the "corrugated" pattern, with the most pronounced corrugation and maximum temperature gradient occurring at the troughs. Significant thermal deformation differences exist at the interface between the rebar cage and concrete, resulting in pronounced internal cracking at this area. No delamination occurred at the interface between the corrugated steel plate and concrete, and the overall deformation of the CSC composite structures remained controllable. This study demonstrates the superior fire resistance of CSC composite structures, aiding in fire protection design for such structures in tunnel engineering and providing guidance for the stability research of tunnel lining structures under fire scenarios.

Keywords: Tunnel engineering, Corrugated steel-concrete composite structures, Fire, Numerical simulation, High-temperature mechanical properties

1. INTRODUCTION

Corrugated steel prefabricated structures have the advantages of good load-bearing performance, strong cross-sectional bending resistance, light weight and easy assembly, fast construction speed, adaptability to various cross-sections, recyclability for reuse, and environmental friendliness (Che et al, 2021). They are widely used in tunnel sheds, connecting passages, shafts, inclined shafts, water conveyance tunnels, and comprehensive pipe galleries (Figure 1). In recent years, the application of corrugated steel plates in tunnel support structures has gradually increased, and scholars have conducted relevant research on their mechanical properties. Such as the analysis of the monitoring laws of corrugated steel shed tunnel structures, the research on the construction technology of corrugated steel prefabricated initial support structures in tunnels, the study on the influence of corrosion on the

[1] PhD, Lei Bo, Civil Engineering, Department of Geotechnical Engineering, College of Civil Engineering, Tongji University, 1239 Siping Road & Key Laboratory of Geotechnical and Underground Engineering, Ministry of Education, Shanghai, 200092, China, 2111001@tongji.edu.cn
[2] Prof., Ding Wenqi, Civil Engineering, Department of Geotechnical Engineering, College of Civil Engineering, Tongji University, 1239 Siping Road & Key Laboratory of Geotechnical and Underground Engineering, Ministry of Education, Shanghai, 200092, China, dingwq@tongji.edu.cn
[3] Assoc. Prof., Zhang Qingzhao, Civil Engineering, Department of Geotechnical Engineering, College of Civil Engineering, Tongji University, 1239 Siping Road & Key Laboratory of Geotechnical and Underground Engineering, Ministry of Education, Shanghai, 200092, China, zhangqingzhao@tongji.edu.cn

performance of buried corrugated steel culverts, and the research on the mechanical properties of corrugated steel prefabricated panels used in the repair of shield tunnel segments, etc (Nakhostin et al, 2022; Yu et al, 2020).

In order to enhance the structural bearing capacity, corrugated steel plates are often combined with concrete to form corrugated steel-concrete composite structures, which have been gradually promoted and applied in tunnel engineering. Due to the frequent occurrence of tunnel fires, the study on the high-temperature mechanical properties of tunnel lining structures has gradually increased in recent years ((Morovat Mohammed A. and Engelhardt Michael D., 2020; Shaheen et al, 2020). Many scholars have conducted relevant experimental and theoretical studies on the mechanical properties of steel at high temperatures (Jiang et al, 2020; Sun et al, 2022). For common steel, strength exhibits a significant decline when the ambient temperature reaches 500 °C. At 600 °C, the steel will lose most of its strength and stiffness (Al-Thairy, 2020). Duplex stainless steel has relatively good strength and ductility, and its strength and ductility are superior to those of single-phase austenitic stainless steel or ferritic stainless steel (Jeong et al, 2015). Maraveas and Vrakas (2014) analyzed the temperature field distribution of reinforced concrete sections under different fire temperature rise curves through non-coupled heat transfer transient numerical analysis. Tomar and Khurana (2020) studied the distribution of air in the tunnel and the surface temperature of the tunnel lining under fire conditions with and without fire prevention measures through numerical simulation. Li et al. (2023) investigated the effects of temperature on the shrinkage behavior and hardening slope of steel yield surfaces, establishing a new yield criteria for stainless steel and high-strength alloy steel under temperature influence.

Research findings on the high-temperature thermodynamic behavior of tunnel structures remain relatively scarce at present. Existing studies primarily focus on reinforced concrete lining structures, with limited systematic investigations into the high-temperature fire resistance of steel lining structures. Research on the load-bearing capacity and stability of corrugated steel-concrete composite structures under fire conditions is insufficient, and studies on the high-temperature performance of novel duplex stainless steel corrugated plate structures are even fewer. This paper employs numerical simulation to investigate the load-bearing capacity and deformation characteristics of corrugated steel-concrete composite structures under various temperature conditions and standard heating curve, verifying the excellent fire resistance performance of the composite structures, which has reference significance for engineering design.

(a) Corrugated steel pipe culvert (b) Corrugated steel tunnel lining (c) Corrugated steel shed

Figure 1. *Applications of corrugated steel structures.*

2. NUMERICAL ANALYSIS

2.1. Finite Element Model

In this study, the sequential coupling method is adopted to calculate the thermodynamic coupling behavior of corrugated steel-concrete composite structures at high temperatures. The specific implementation is divided into two steps: Firstly, the distribution result of the temperature field of the corrugated steel-concrete composite structure is calculated based on the fire scene. Then, the calculation result of the temperature field is applied as a boundary condition to the mechanical model to calculate the force and deformation behavior of the structure.

The finite element model is established based on the actual geometric dimensions of the specimen. The wave distance-wave height-thickness of the corrugated steel plate is 380mm-140mm-5mm. The length of the steel plate is 2.40m and the width is 1.24m. The steel grade is the new duplex stainless steel S32001, with a room-temperature elastic modulus E_{cs}=258.86GPa. The plain concrete strength grade is C30, with dimensions matching the corrugated steel plate (length and width) and the thickness of 30 cm. The steel bar grades are all HRB400, with an elastic modulus E_s=200GPa. Among them, the diameter of the longitudinal force-bearing steel bar is 22mm, and

the diameters of the supporting and transverse distributed steel bars are 12mm. The base plate beneath the corrugated steel plate is made of Q235 grade steel.

The corrugated steel plate, concrete, backing plates and loading frames are simulated using three-dimensional solid elements, and the reinforcing bars are all simulated using truss elements. The grid division of each component is shown in Figure 2. The concrete and the steel cage are embedded constraints, the concrete and the corrugated steel plate are in hard contact, the corrugated steel plate and the steel cage are tie constraints, the corrugated steel plate and the base plates are tie constraints, and the concrete and the loading frame are tie constraints. The vertical force is applied to the specimen by the vertical jack through two distribution beams, and the corresponding vertical load is applied at the corresponding position in the finite element model. The horizontal force acts directly on the specimen through the horizontal jack, so the corresponding horizontal load is applied at the center position of the jack's flexible head.

The calculation of the temperature field adopts the transient heat transfer analysis method, which can describe the real-time changes of the temperature field over time. Under actual fire conditions, complex situations such as evaporation of internal moisture in concrete and concrete cracking may occur, making the calculation difficult to achieve. In this study, certain simplifications have been made: (1) The three-dimensional load structure method is adopted for the thermodynamic sequential coupling calculation, considering the heat transfer effects of corrugated steel plate, steel cages and concrete, and the influence of the stratum is treated according to the boundary conditions of heat dissipation and static load; (2) The temperature changes caused by the evaporation of water inside the concrete are not taken into account. (3) The impact of concrete cracking is not analyzed for the time being.

The number of grids in the model is 61450. In the pure thermal calculation example, the element types of corrugated steel plate, concrete, backing plates and loading frames are DC3D8R, and the element type of the steel cage is DC1D2. In the mechanical calculation example, the unit types of corrugated steel plate, concrete, backing plates and loading frames are C3D8R, and the unit type of the steel cage is T3D2.

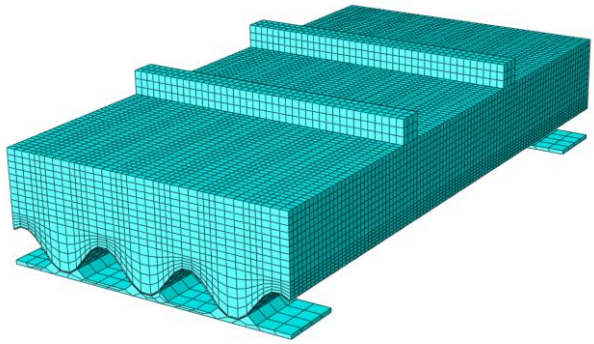

Figure 2. *Three-dimensional finite element calculation model.*

2.2. Material Parameters

In thermodynamic simulation, it is necessary to determine the thermodynamic parameters of the materials. In the process of taking values for the thermodynamic parameters of the materials, this paper references the "Eurocode 2: Design of concrete structures, EN 1992-1-2" and "Eurocode 3: Design Of Steel Structures-Part 1-2: General Rules-Structural Fire Design".

(1) Thermal parameters of steel

Table 1 presents the thermal parameters of steel, including the coefficient of thermal expansion, thermal conductivity, specific heat capacity and density.

Table 1. *Thermal parameters of steel.*

Parameters	Symbol	Value	Unit
Coefficient of thermal expansion	α_s	1.4×10^{-5}	m/(m·℃)
Thermal conductivity coefficient	λ_s	45	W/(m·℃)
Specific heat capacity	c_s	600	J/(kg·℃)
Density	ρ_s	7850	kg/m³

(2) High-temperature mechanical parameters of steel

1) Elastic modulus

The elastic modulus at different temperatures is calculated according to Equations (1) and (2):

$$E_{sT} = \chi_{sT} E_s \tag{1}$$

$$\chi_{sT} = \begin{cases} \dfrac{7T-4780}{6T-4760} & (20^\circ\mathrm{C} \le T \le 600^\circ\mathrm{C}) \\ \dfrac{1000-T}{6T-2800} & (600^\circ\mathrm{C} \le T \le 1000^\circ\mathrm{C}) \end{cases} \tag{2}$$

In the formula, E_{sT} is the elastic modulus value of steel at high temperature; E_s is the elastic modulus value of steel at room temperature, and χ_{sT} is the elastic modulus reduction coefficient of steel at high temperature.

2) Material strength

The strength at different temperatures is calculated according to Equations (3) and (4):

$$f_{sT} = \eta_{sT} f_s \tag{3}$$

$$\eta_{sT} = \begin{cases} 1.0 & (20^\circ\mathrm{C} \le T \le 300^\circ\mathrm{C}) \\ 1.24\times10^{-8}T^3 - 2.096\times10^{-8}T^2 & \\ +9.228\times10^{-3}T - 0.2168 & (300^\circ\mathrm{C} \le T \le 800^\circ\mathrm{C}) \\ 0.5 - T/2000 & (800^\circ\mathrm{C} \le T \le 1000^\circ\mathrm{C}) \end{cases} \tag{4}$$

In the formula, f_{sT} is the strength value of steel at high temperature, and f_s is the strength value of steel at room temperature, and η_{sT} is the strength reduction coefficient of steel at high temperature.

(3) Thermal parameters of concrete

1) Density and coefficient of thermal expansion: The density of concrete is taken as 2300kg/m ³, and the coefficient of thermal expansion of concrete is taken as $\alpha_c = 1.8\times10^{-5}\ \mathrm{m/(m\cdot{}^\circ C)}$.

2) Thermal conductivity λ_c: The unit of thermal conductivity is W/(m·℃), and its value varies with temperature T as follows:

$$\lambda_c = 1.68 - 0.19\frac{T}{100} + 0.0082\left(\frac{T}{100}\right)^2 \tag{5}$$

3) Specific heat capacity: The unit of specific heat capacity is J/(kg·℃), and the relationship between specific heat capacity and temperature T is taken as follows:

$$c_c = 890 + 56.2\frac{T}{100} - 3.4\left(\frac{T}{100}\right)^2 \tag{6}$$

(4) High-temperature mechanical parameters of concrete

The calculation formulas for the elastic modulus and axial compressive strength of ordinary concrete under high-temperature conditions are as follows:

$$E_{cT} = \chi_{cT} E_c \tag{7}$$

$$f_{cT} = \eta_{cT} f_c \tag{8}$$

In the formula , E_{cT} is the elastic modulus value of concrete at high temperature, E_c is the elastic modulus value of concrete at room temperature, and χ_{cT} is the elastic modulus reduction coefficient of concrete at high temperature. f_{cT} is the axial compressive strength value of concrete at high temperature, and f_c is the axial compressive strength value of concrete at room temperature. η_{cT} is the axial compressive strength value reduction coefficient of concrete at high temperature. Table 2 shows axial compressive strength and elastic modulus reduction coefficient of ordinary concrete at high temperature.

Table 2. *Axial compressive strength and elastic modulus reduction coefficient of ordinary concrete at high temperature.*

T/℃	**20**	**100**	**200**	**300**	**400**	**500**	**600**	**700**	**800**	**900**	**1000**	**1100**
χ_{cT}	1.0	0.625	0.432	0.304	0.188	0.1	0.045	0.03	0.015	0.008	0.004	0.001
η_{cT}	1.0	1.00	0.95	0.85	0.75	0.6	0.45	0.30	0.15	0.08	0.04	0.01

2.3. Load Conditions

The load conditions in this paper are mainly divided into two parts. The first part is the high-temperature mechanical analysis of corrugated steel-concrete composite structures at different temperatures. Corresponding overall uniform temperature field boundary conditions are applied to the composite structures under different temperature conditions. The temperature value range under the high-temperature condition is 100 ℃ to 500 ℃, and one condition is calculated at intervals of 100 ℃. There are a total of five conditions. Each working condition lasts for 2 hours. The axial force of the composite structure is 600KN and the vertical force is 1000KN.

The second part is that the specimen is heated for 2 hours on the ISO834 heating curve, accompanied by mechanical loading. The axial force of the composite structure is 600KN and the vertical force is 1000KN to explore the high-temperature mechanical properties of the composite structure. Figure 3 shows the typical fire temperature rise curves, where the formula of the ISO834 temperature rise curve is shown as Equation (9) :

$$T = 345\lg(8t+1)+20 \tag{9}$$

In the formula, T represents the temperature in the fire environment and t represents the duration of the fire.

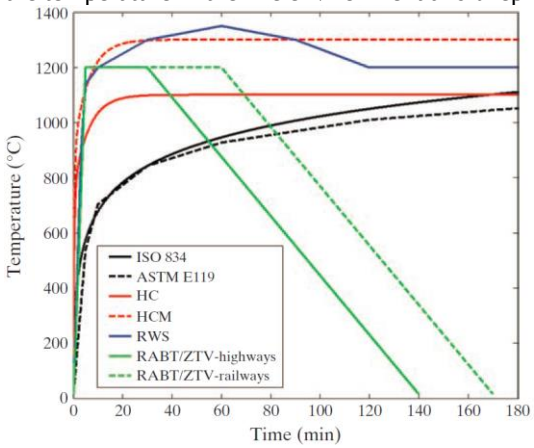

Figure 3. *Typical temperature rise curves.*

3. NUMERICAL SIMULATION RESULTS AT DIFFERENT TEMPERATURES

3.1. Displacement varies with time at different temperatures

From the numerical simulation results, the vertical displacement cloud maps of each temperature condition lasting for 1 hour and 2 hours are extracted, and the graphs of vertical displacement varying with time under different temperature conditions are drawn, as shown in Figs. 4 and 5. As shown in Figs. 4 and 5, the deformation of the corrugated steel-concrete composite structure under different temperature working conditions is relatively similar. The upper part of the structure is under compression and the lower part is under tension. The overall structure bends upward. At the same time, the vertical displacement increases with the increase of temperature. The maximum mid-span vertical displacements of the composite structure maintained for 1 hour at temperatures of 100 ℃, 200 ℃, 300 ℃, 400 ℃ and 500 ℃ are 0.657mm, 0.9mm, 1.207mm, 1.779mm and 3.013mm, respectively. The maximum mid-span vertical displacements of the composite structure maintained for 2 hours at temperatures of 100 ℃, 200 ℃, 300 ℃, 400 ℃ and 500 ℃ for 2 hours are 1.357mm, 1.868mm, 2.544mm, 3.890mm and 7.051mm, respectively. The mid-span vertical displacement ratios of the composite structure maintained at temperatures of 100 ℃, 200 ℃, 300 ℃, 400 ℃ and 500 ℃ for 2 hours and 1 hour are 2.065, 2.076, 2.108, 2.187 and 2.34, respectively. It can be known that with the increase of time, the influence of different temperatures on the deformation of the composite structure shows regularity.

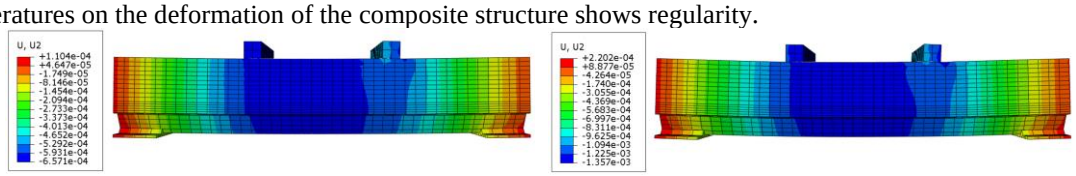

(a) 100℃-1h (b) 100℃-2h

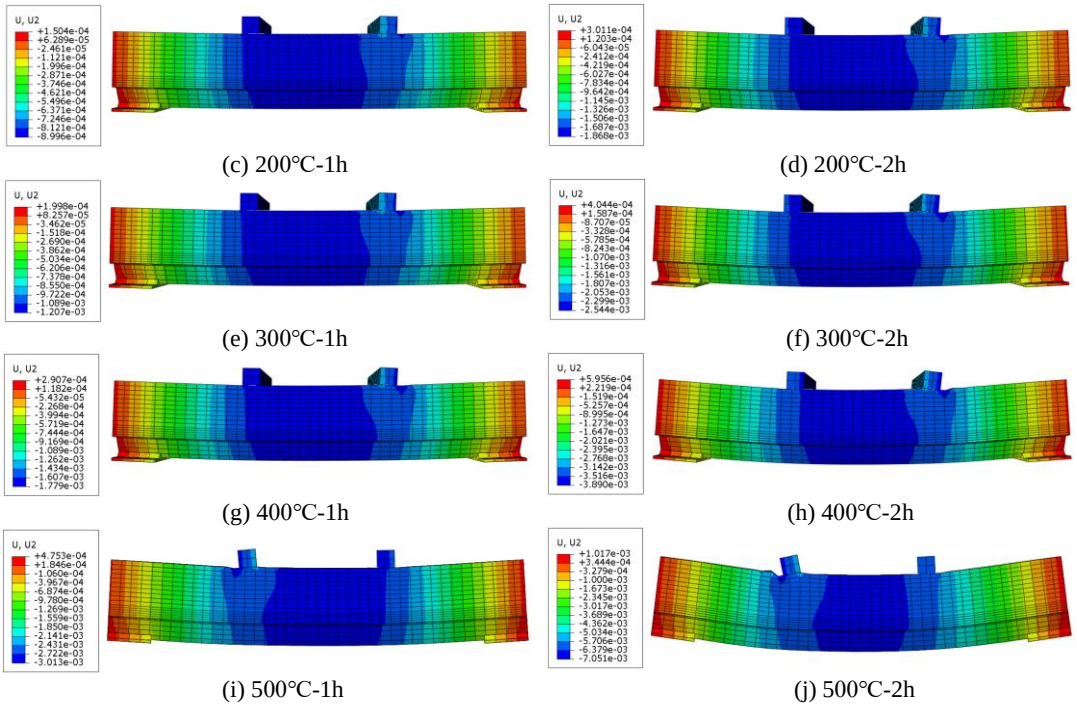

(c) 200℃-1h (d) 200℃-2h

(e) 300℃-1h (f) 300℃-2h

(g) 400℃-1h (h) 400℃-2h

(i) 500℃-1h (j) 500℃-2h

Figure 4. *Displacement variation with time at different temperatures (Unit: m, deformation magnified 15 times).*

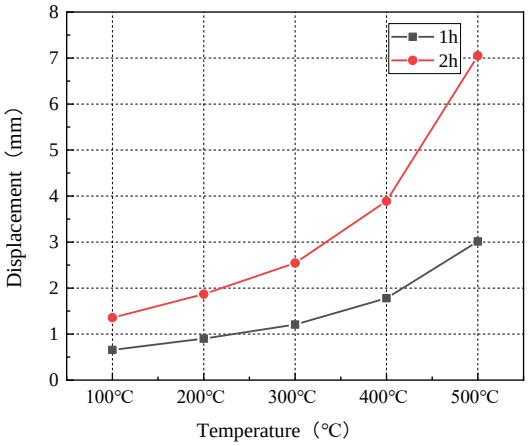

Figure 5. *Graph of vertical displacement varying with time under different temperature conditions.*

3.2. Stress variations with time at different temperatures

From the numerical simulation results, the Mises stress cloud diagrams of each temperature condition lasting for 1 hour and 2 hours are extracted (Figure 6). As shown in Figure 6, the maximum Mises stresses for the composite structure maintained at 100 °C, 200 °C, 300 °C, 400 °C, and 500 °C for 2 hours are 195.8 MPa, 209.5 MPa, 225 MPa, 252.2 MPa, and 279.4 MPa, respectively. Stress levels increased with rising temperature and prolonged duration.

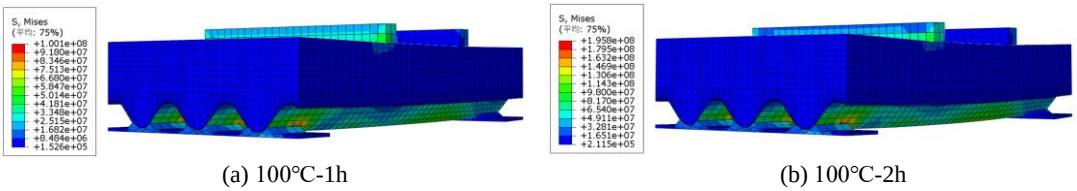

(a) 100℃-1h (b) 100℃-2h

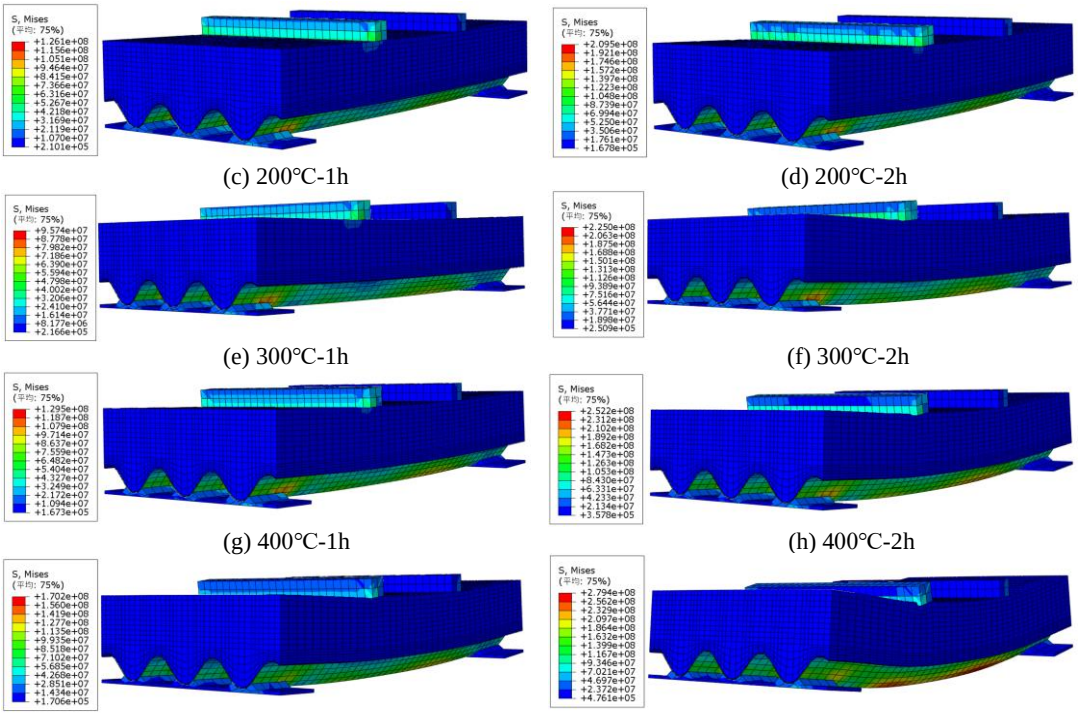

(c) 200℃-1h (d) 200℃-2h

(e) 300℃-1h (f) 300℃-2h

(g) 400℃-1h (h) 400℃-2h

(i) 500℃-1h (j) 500℃-2h

Figure 6. *Stress variation over time at different temperatures (Unit: Pa, deformation amplification 15 times).*

4. NUMERICAL SIMULATION RESULTS UNDER THE ISO834 TEMPERATURE RISE CURVE

4.1. Temperature field distribution varies with time

The temperature field distribution of the whole composite structure, concrete, steel cage and corrugated steel plate with time after heating for 1 hour under the ISO834 heating curve is shown in Figure 7. As shown in Fig. 7(c)~(d), the maximum temperatures of the corrugated steel plate reach 946 °C and 1047 °C after 1 hour and 2 hours of heating, respectively. The trough temperature is higher than the peak temperature, and the temperature field distribution along the longitudinal direction of the specimen is consistent.

As shown in Fig. 7(e)~(f), the temperature field at the bottom of the concrete is similar to that of the corrugated steel plate. Due to the low thermal conductivity and large specific heat capacity of the concrete material, the overall heating rate of the concrete is significantly slower than that of the steel. After 1 hour and 2 hours of heating, the maximum concrete temperatures reach 798 °C and 886 °C, respectively, demonstrating significant thermal inertia. The cross-sectional temperature field distribution along the thickness direction of the concrete shows a "wavy" feature. The closer it is to the trough, the more obvious the wavy feature becomes. From 1 hour to 2 hours, the corrugated cloud pattern of the cross-section gradually expands upwards. The thickness of the concrete affected by fire gradually increases, the overall temperature keeps rising, and the temperature gradient keeps increasing.

As shown in Fig. 7(g)~(h), the temperature difference between the bottom of the stiffening ribs and the adjacent corrugated steel plate is relatively small. After 1 hour and 2 hours of heating, the temperatures at this location reach 852 °C and 946 °C, respectively, exceeding the temperature of the underlying concrete in contact with the corrugated steel plate. The temperature of the stiffening ribs gradually decreases from bottom to top. The upper transverse and longitudinal bars are far away from the heating surface and have a lower temperature. Moreover, as the heating duration increases, the temperature beneath the stiffening ribs rises significantly, while the temperature of the upper ribs shows little change, resulting in a continuously widening temperature gradient within the stiffening ribs. Due to the different thermal parameters of the steel cage and the concrete, the amount of thermal deformation at the contact part between the steel cage and the concrete varies, resulting in deformation misalignment between the two. Moreover, as the temperature rises, the internal damage of the concrete increases, and the concrete at the contact point with the steel cage experiences significant stress, leading to notable internal cracks.

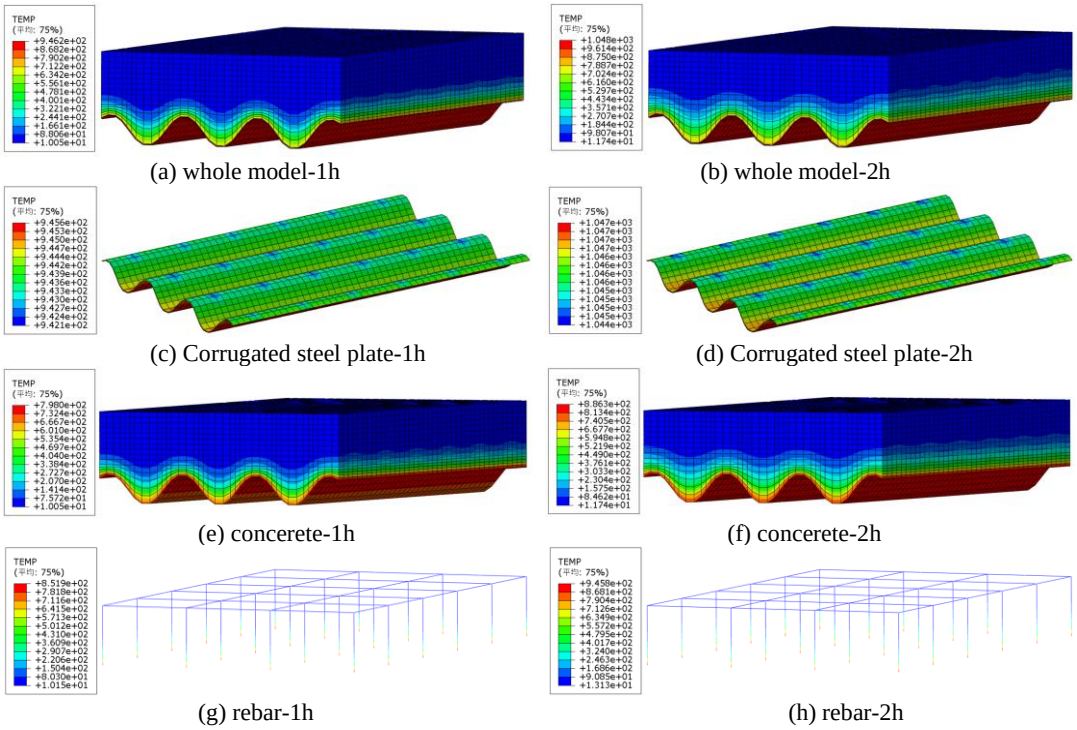

(a) whole model-1h (b) whole model-2h

(c) Corrugated steel plate-1h (d) Corrugated steel plate-2h

(e) concerete-1h (f) concerete-2h

(g) rebar-1h (h) rebar-2h

Figure 7. *The temperature field distribution of the specimen under ISO834 heating curve*

(Unit: ℃, deformation magnified 15 times).

4.2. Displacement varies with time

From the numerical simulation results, the vertical displacement cloud maps of heating for 1 hour and 2 hours under the ISO834 heating curve are extracted, as shown in Figure 8. It can be known from Figure 8 that under the ISO834 heating curve, the upper part of the corrugated steel-concrete composite structure is compressed and the lower part is tensioned, and the overall structure bends upward. The composite structure exhibited maximum mid-span vertical displacements of 4.035 mm and 13.27 mm after 1 hour and 2 hours of heating, respectively.Also, the vertical displacements increased significantly with the increase of heating time.

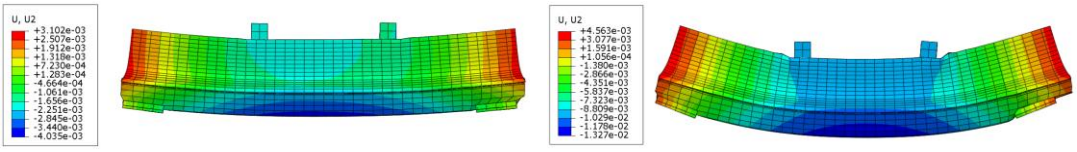

(a) 1h (b) 2h

Figure 8. *The displacement of the specimen under ISO834 temperature rise curve varies with time*

(Unit: m, deformation magnified 15 times).

4.3. Stress varies with time

To observe the stress distribution of the corrugated steel-concrete composite structure during the fire exposure process, the stress cloud diagrams corresponding to the composite structure, concrete, steel cage and corrugated steel plate at 1 hour and 2 hours of fire exposure are extracted respectively, as shown in Figure 9. It can be seen from Figure 9 that the stress on the upper part of the concrete and the upper part of the wave crest is relatively large, and the stress on the longitudinal bars at the upper part of the steel cage and the bars at the upper part of the wave crest is also relatively large, and all the stresses keep increasing over time. As shown in Fig. 9(g)~(h), when the fire exposure time reaches 1 hour and 2 hours, the temperature of the corrugated steel plate has approached 1000 ℃. At this temperature, the yield strength of the corrugated steel is 18.3MPa. The corrugated steel shows a large area of yield, and the stress at the wave crest is significantly higher than that at the wave trough. A significant stress concentration phenomenon also occurs at the welding area between the bottom corrugated steel plate and backing plates. This is primarily due to the continued use of existing Q235 carbon steel bearing plates in this

calculation example. Differences in thermodynamic parameters between the bearing material and the new duplex stainless steel corrugated steel lead to variations in thermal deformation between the two materials, resulting in stress concentration at their contact areas.

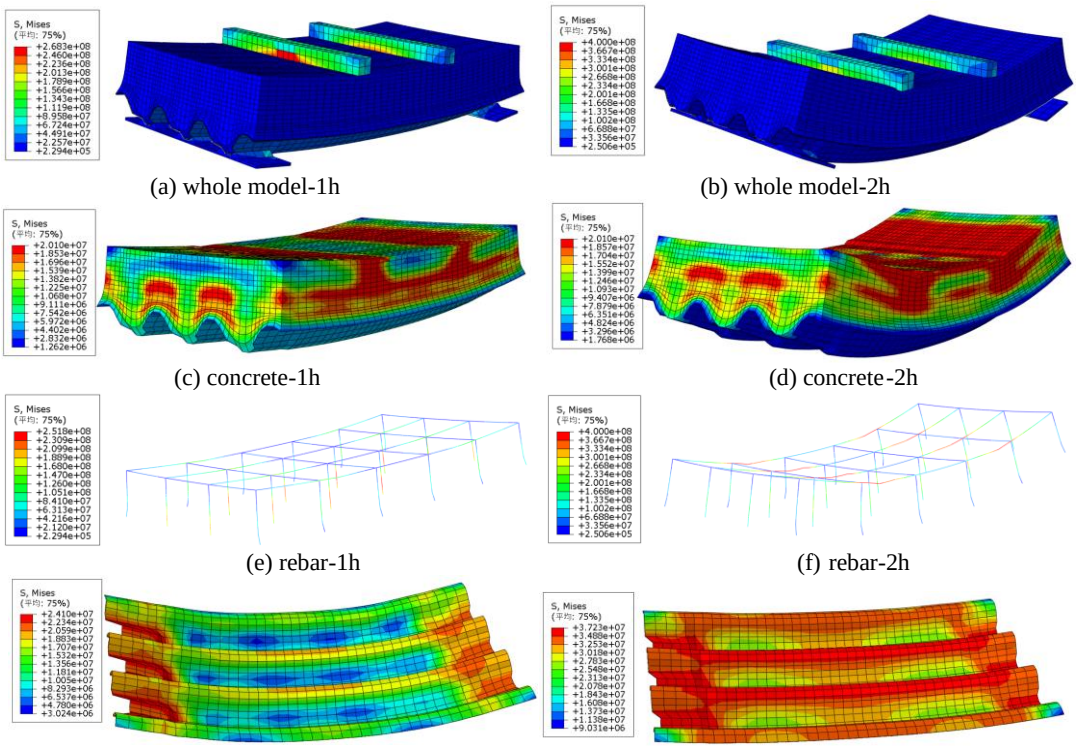

Figure 9. *The stress of the specimen varies with time under the ISO834 heating curve (Unit: Pa, deformation amplification 15 times).*

5. CONCLUSIONS

In this study, numerical simulation methods are adopted to analyze the bearing capacity and deformation characteristics of corrugated steel-concrete composite structures under different temperature conditions and ISO heating curves, and the following conclusions are obtained:

(1) The deformation of corrugated steel-concrete composite structures under temperature conditions ranging from 100 ℃ to 500 ℃ is relatively similar. The upper part of the structure is under compression, the lower part is under tension, and the overall structure bends upward. The vertical displacement and stress level increase with the rise in temperature and the passage of time.

(2) Under the ISO834 heating curve, the maximum temperature of the corrugated steel plate after 2 hours of heating is 1047 ℃, and the trough temperature is higher than the peak temperature. The temperature field distribution of the steel plate is consistent along the longitudinal distribution of the specimen. The temperature field distribution of the specimen cross-section shows a "wavy" feature. The closer it is to the trough, the more obvious the wavy feature becomes. The temperature is the highest and the temperature gradient is the greatest at the trough. There is a significant difference in the amount of thermal deformation at the contact part between the steel cage and the concrete, which can lead to obvious internal cracks at this location.

(3) Under the ISO834 heating curve, both the vertical displacement and stress of the corrugated steel-concrete composite structure keep increasing over time. After being exposed to fire for 2 hours, the corrugated steel plate shows a relatively large area of yield, but the overall deformation of the composite structure is within the allowable range.

Our research group has conducted the full-scale fire test on corrugated steel-concrete composite structures under the ISO 834 heating curve. The corrugated steel-concrete composite structure maintains stability under simultaneous fire heating and mechanical loading, with no delamination observed at the interface between the corrugated steel plate and concrete. This validates the excellent fire resistance of this composite structure. Subsequent work will involve stability verification and fire-resistance design for corrugated steel-lined tunnels under fire scenarios, based on test results, numerical simulations, and theoretical analysis.

6. ACKNOWLEDGMENTS

The authors wish to acknowledge the sponsorship from the National Natural Science Foundation of China(NO.52378405), the Major Science and Technology Special Project of Yunnan Provincial Department of Transportation(No.202302AD080007), and "Transportation Science and Technology Demonstration Project of the Ministry of Transport: Intelligent Construction Science and Technology Demonstration Project of Complex Environment Tunnels along the Jinsha River Expressway in Yunnan Province".

7. REFERENCES

[1] Al-Thairy, H. (2020). A simplified method for steady state and transient state thermal analysis of hybrid steel and FRP RC beams at fire. Case Studies in Construction Materials, 13, e00465. https://doi.org/10.1016/j.cscm.2020.e00465
[2] Che, H., Tong, L., Liu, S., Yang, Q. (2021). Field investigation on the mechanical performance of corrugated steel utility tunnel (CSUT). Journal of Constructional Steel Research, 183, 106693. https://doi.org/10.1016/j.jcsr.2021.106693
[3] Jeong, C. U., Heo, Y.-U., Choi, J. Y., Woo, W., Choi, S.-H. (2015). A study on the micromechanical behaviors of duplex stainless steel under uniaxial tension using ex-situ experimentation and the crystal plasticity finite element method. International Journal of Plasticity, 75, 22–38. https://doi.org/10.1016/j.ijplas.2015.07.005
[4] Jiang, S., Zhu, S., Guo, X., Chen, C., Li, Z. (2020). Safety monitoring system of steel truss structures in fire. Journal of Constructional Steel Research, 172, 106216. https://doi.org/10.1016/j.jcsr.2020.106216
[5] Li, S., Ding, W., Zhang, Q. (2023). Development of a new temperature-dependent yield criterion for stainless and high-strength alloy steels in construction engineering. Case Studies in Construction Materials, 18, e02149. https://doi.org/10.1016/j.cscm.2023.e02149
[6] Maraveas, C., and Vrakas, A. A. (2014). Design of Concrete Tunnel Linings for Fire Safety. Structural Engineering International, 24(3), 319–329. https://doi.org/10.2749/101686614X13830790993041
[7] Morovat Mohammed A. and Engelhardt Michael D. (2020). Critical Review of Test Methods for Mechanical Characterization of Steel for Structural-Fire Engineering Applications. Journal of Structural Engineering, 146(11), 04020228. https://doi.org/10.1061/(ASCE)ST.1943-541X.0002787
[8] Nakhostin, E., Kenny, S., Sivathayalan, S. (2022). A numerical study of erosion void and corrosion effects on the performance of buried corrugated steel culverts. Engineering Structures, 260, 114217. https://doi.org/10.1016/j.engstruct.2022.114217
[9] Shaheen, M. A., Foster, A. S. J., Cunningham, L. S., Afshan, S. (2020). Behaviour of stainless and high strength steel bolt assemblies at elevated temperatures—A review. Fire Safety Journal, 113, 102975. https://doi.org/10.1016/j.firesaf.2020.102975
[10] Sun, G., Li, Z., Wu, J., Ren, J. (2022). Investigation of steel wire mechanical behavior and collaborative mechanism under high temperature. Journal of Constructional Steel Research, 188, 107039. https://doi.org/10.1016/j.jcsr.2021.107039
[11] Tomar, M. S., and Khurana, S. (2020). A numerical study on the influence of different tunnel lining insulation materials in a road tunnel fire. Materials Today: Proceedings, 28, 665–671. https://doi.org/10.1016/j.matpr.2019.12.274
[12] Yu, C., Ding, W., Wu, T., Zhang, Q. (2020). Study on calculation method of new corrugated steel reinforcement structure of highway tunnel. IOP Conference Series: Materials Science and Engineering, 741(1), 012073. https://doi.org/10.1088/1757-899X/741/1/012073
[13] (CEN) European Committee for Standardization. Eurocode 2: Design of concrete structures, EN 1992-1-2 [S]. 2004.
[14] Standardization European Committee For. Eurocode 3: Design Of Steel Structures - Part 1-2: General Rules - Structural Fire Design [S]. 2005.